J. Fluid Mech. (2002), *vol.* 467, *pp.* 269–287.
DOI: 10.1017/S0022112002001362 Printed in the United Kingdom

A weakly nonlinear model of long internal waves in closed basins

By D. A. HORN[1], J. IMBERGER[1], G. N. IVEY[1] AND L. G. REDEKOPP[2]

[1]Centre for Water Research, The University of Western Australia, Crawley, WA 6009, Australia

[2]Department of Aerospace and Mechanical Engineering, University of Southern California, Los Angeles, CA 90089-1191, USA

(Received 27 March 2000 and in revised form 11 November 2001)

A simple model is developed, based on an approximation of the Boussinesq equation, that considers the weakly nonlinear evolution of an initial interface disturbance in a closed basin. The solution consists of the sum of the solutions of two independent Korteweg–de Vries (KdV) equations (one along each characteristic) and a second-order wave–wave interaction term. It is demonstrated that the solutions of the two independent KdV equations over the basin length $[0, L]$ can be obtained by the integration of a single KdV equation over the extended reflected domain $[0, 2L]$. The main effect of the second-order correction is to introduce a phase shift to the sum of the KdV solutions where they overlap. The results of model simulations are shown to compare qualitatively well with laboratory experiments. It is shown that, provided the damping timescale is slower than the steepening timescale, any initial displacement of the interface in a closed basin will generate three types of internal waves: a packet of solitary waves, a dispersive long wave and a train of dispersive oscillatory waves.

1. Introduction

It is well established (e.g. Mortimer 1952) that wind blowing over a lake results in a tilt of the free surface, upward at the leeward shore, and a corresponding downward tilt of the thermocline within the fluid. When the wind stress is removed, the free surface and the thermocline relax, generating basin-scale long waves at each interface: the surface and internal seiches. Understanding the dynamics of the internal seiche is important as it is a source of kinetic energy for driving transport and mixing in lakes (Imberger 1998).

Historically, analysis of the internal seiche has been based on linear theory (e.g. Mortimer 1952; Heaps & Ramsbottom 1966; Spigel & Imberger 1980), usually assuming a simple two-layer density structure. However, field observations have shown that the amplitude of the internal seiche is often large enough to allow nonlinear effects to become significant (e.g. Thorpe, Hall & Crofts 1972; Hunkins & Fliegel 1973; Farmer 1978; Wiegand & Carmack 1986).

Numerical modelling has demonstrated the importance of nonlinear effects in the generation of small-scale features observed in the internal wave field in lakes (Hutter *et al.* 1998). Furthermore, it has been shown that nonlinear steepening is expected to be an important mechanism in the degeneration of basin-scale internal waves in most lakes (Horn, Imberger & Ivey 2001).

The nonlinear steepening of an initial seiche leads to the generation of an internal surge, or packet of solitons, so that energy is transferred within the internal wave spectrum from the basin-scale to much shorter lengthscales. Horn *et al.* (2001) conducted a series of laboratory experiments with vertical endwalls but postulated that this transfer of energy from the seiche to solitons has important implications for boundary mixing in lakes because solitons are likely to shoal at sloping boundaries. To investigate the degeneration of large-scale internal waves in closed basins, such as in either the laboratory experiments of Horn *et al.* (2001) or in a lake, we develop here a simple model to simulate the nonlinear steepening of an initial basin-scale internal wave and the subsequent evolution and propagation of solitons.

The simplest model to include weak nonlinearity is the Korteweg–de Vries (KdV) equation (for a general review of the KdV equation see Miles 1981). The KdV equation describes the evolution of waves that are long compared with both their amplitude and the total depth of the fluid and assumes that nonlinear effects enter the equations at the same order as dispersive effects. In a simple inviscid two-layer system consisting of a fluid with density ρ_1 and depth h_1 overlying a fluid of density ρ_2 and depth h_2, and making the Boussinesq approximation, the KdV equation can be written as

$$\eta_t + c_0\eta_x + \alpha\eta\eta_x + \beta\eta_{xxx} = 0, \tag{1.1}$$

where $\eta(x,t)$ is the interface displacement, $c_0 = (g'h_1h_2/H)^{1/2}$ is the linear long-wave speed, $g' = (\Delta\rho/\rho_0)g$, $\alpha = \frac{3}{2}c_0(h_1 - h_2)/h_1h_2$ and $\beta = \frac{1}{6}c_0h_1h_2$. Several modified KdV-type equations have also been derived that extend the range over which this type of equation can be applied as well as allowing for the inclusion of slow variations in depth, stratification and background shear (e.g. Djordjevic & Redekopp 1978; Maslowe & Redekopp 1980; Helfrich, Melville & Miles 1984). The equation and its modified forms have been applied to observations in lakes and coastal seas (e.g. Hunkins & Fliegel 1973; Lee & Beardsley 1974; Sandstrom & Elliott 1984) and shown to agree well with experimental data (e.g. Koop & Butler 1981; Segur & Hammack 1982).

The KdV equation is unidirectional, however, and considers the slow time evolution of a long wave as it propagates along only one characteristic. In many instances this does not matter, but it does neglect the possibility of the interaction of waves travelling in opposite directions as can occur in closed basins for example. In a simple two-dimensional domain such as a laboratory tank or long narrow lake, an arbitrary initial disturbance will evolve into waves propagating in opposite directions, but only the evolution and interaction of long waves moving in one direction can be described by a single KdV equation. As these waves are reflected from the boundaries of a confined basin, they will necessarily pass through one another in opposite directions, an interaction that cannot be described by the KdV equation.

The aim of this paper is to introduce a simple computational model that describes the weakly nonlinear evolution of an initial disturbance and its subsequent reflection from the boundaries of a closed basin such as a laboratory tank or idealized lake. We begin by describing an approach which employs a virtual reflected domain that advantageously allows the approximate computation of the wave field composed of information propagating along both characteristics via the integration of a single KdV equation with a second-order correction. Dissipative effects arising from wave-induced boundary layers are introduced into the model and the results of model simulations and laboratory experiments are compared. We then briefly examine the internal waves that are generated by a tilted interface in a closed basin, describing

the wave field in terms of known solutions to the KdV equation. The generation of relatively short waves is shown to have important implications for boundary mixing in lakes.

2. Proposed weakly nonlinear model

2.1. *Method of solution by reflection*

We are interested in the evolution of the internal wave field arising from an initial disturbance of the interface in a two-layer system in a closed basin of uniform depth. The starting point for our analysis is the Boussinesq equation (Redekopp 2000; New & Pingree 2000) written in unscaled coordinates:

$$\mathscr{N}_{tt} - c_0^2 \mathscr{N}_{xx} = \tfrac{1}{3} c_0^2 h_1 h_2 \mathscr{N}_{xxxx} + \frac{h_1 - h_2}{h_1 h_2} (2\mathscr{N}_t \mathscr{N}_{xt} + c_0^2 \mathscr{N}_x \mathscr{N}_{xx}), \tag{2.1}$$

where the interfacial displacement is given by $\eta(x,t) = \mathscr{N}_x$. This equation is derived from the Euler equations by employing a similar asymptotic expansion to that used in obtaining the KdV equation (1.1) (i.e. weak nonlinearity balanced by weak dispersive effects) except for one very important difference: any bias toward propagation along a given characteristic has been specifically avoided in (2.1).

The d'Alembert solution of the linear wave equation appearing on the left-hand side of (2.1) for an initial displacement of the interface $\eta_0(x)$ is composed of identical waves of amplitude $\eta_0/2$, one moving to the right along the characteristic $\mathrm{d}x/\mathrm{d}t = c_0$ and the other moving to the left along $\mathrm{d}x/\mathrm{d}t = -c_0$. In a closed basin of length L, the waves will reflect from the endwalls where their directions will be reversed (see figure 1). We will assume here that the endwalls are vertical and perfectly reflecting, a good approximation of the laboratory tank.

Our goal in this section is to develop an approximate and practically useful solution procedure for the bi-directional evolution in $[0, L]$ defined by (2.1). We introduce the slow independent variables $(X, T) = \mu(x, t)$, where $\mu = h/\lambda$ is the long-wave parameter. Similarly, we introduce an amplitude parameter $\epsilon = a/h$ and use the KdV scaling $\epsilon = \mu^2$ so that the effects of dispersion and nonlinearity balance. We now consider an asymptotic representation of the solution of (2.1) having the form

$$\mathscr{N}(x,t) = \frac{\epsilon}{\mu} \{ \mathscr{N}^{(1)}(X,T) + \epsilon \mathscr{N}^{(2)}(X,T) + \epsilon^2 \mathscr{N}^{(3)}(X,T) + \cdots \}, \tag{2.2}$$

for the initial value problem with $\eta(x,0) = \eta_0(x)$.

As anticipated, the leading-order balance equation resulting from the expansion (2.2) is simply the linear wave equation

$$\mathscr{N}^{(1)}_{TT} - c_0^2 \mathscr{N}^{(1)}_{XX} = 0, \tag{2.3}$$

which possesses the fundamental (d'Alembert) solution

$$\mathscr{N}^{(1)}(X,T) = F(r,\tau) + G(s,\tau). \tag{2.4}$$

The independent variables r and s are characteristic coordinates

$$r = X - c_0 T, \quad s = X + c_0 T, \tag{2.5}$$

and $\tau = \epsilon T$ is a slow timescale required to enforce consistency in the asymptotic expansion (2.2).

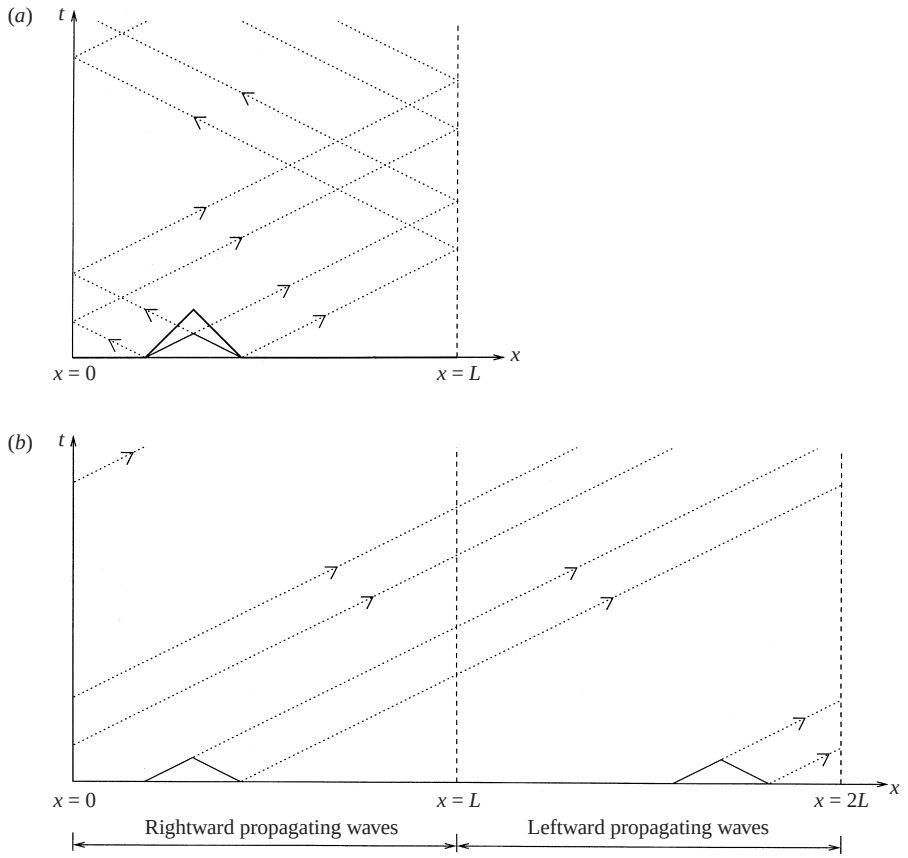

FIGURE 1. Schematic representation of the reflected domain. (*a*) Any initial condition will evolve into leftward and rightward propagating waves that will change direction on reflection from the vertical boundaries at $x = 0, L$. (*b*) This system can be represented in a uni-directional domain with periodic boundary conditions at $x = 0, 2L$ in which rightward propagating waves are represented in $[0, L]$ and leftward propagating waves in $[L, 2L]$. Whereas a rightward propagating wave in the bi-directional domain is reflected from the end of the tank at $x = L$ and becomes a leftward propagating wave, in the new domain the wave continues from $[0, L]$ into $[L, 2L]$ (which represents leftward propagating waves). Similarly, due to the periodic boundary conditions, on reaching $x = 2L$ the wave reappears at $x = 0$, changing from leftward to rightward propagating in exactly the same way as a wave reflected from the left boundary ($x = 0$) in the bi-directional domain.

The next order balance yields the inhomogeneous equation

$$2c_0\frac{\partial^2\mathcal{N}^{(2)}}{\partial r\partial s} = -\frac{\partial}{\partial r}\left\{F_\tau + \tfrac{3}{4}c_0\frac{h_1-h_2}{h_1h_2}F_r^2 + \tfrac{1}{6}c_0h_1h_2F_{rrr}\right\} + \frac{\partial}{\partial s}\left\{G_\tau - \tfrac{3}{4}c_0\frac{h_1-h_2}{h_1h_2}G_s^2 + \tfrac{1}{6}c_0h_1h_2G_{sss}\right\} + \frac{c_0}{2}\frac{h_1-h_2}{h_1h_2}(F_rG_{ss} + F_{rr}G_s). \tag{2.6}$$

Clearly, the first two bracketed terms on the right-hand side must vanish separately in order to avoid the appearance of secular behaviour in the solution for $\mathcal{N}^{(2)}$. Hence, we find that $F(r, \tau)$ and $G(s, \tau)$, the independent d'Alembert solutions, satisfy separate, uncoupled KdV equations. Recalling that the dimensional interface displacement is

$\eta = \mathscr{N}_x$, one arrives at the relations

$$\eta(x,t) = \epsilon\eta^{(1)}(X,T,\tau) + \epsilon^2\eta^{(2)}(X,T,\tau) + \cdots, \tag{2.7}$$

$$\eta^{(1)} = \frac{\partial \mathscr{N}^{(1)}}{\partial X} = F_r + G_s = f(r,\tau) + g(s,\tau), \tag{2.8}$$

$$f_\tau + \tfrac{3}{2}c_0\frac{h_1 - h_2}{h_1 h_2} f f_r + \tfrac{1}{6}c_0 h_1 h_2 f_{rrr} = 0, \tag{2.9}$$

$$g_\tau - \tfrac{3}{2}c_0\frac{h_1 - h_2}{h_1 h_2} g g_s - \tfrac{1}{6}c_0 h_1 h_2 g_{sss} = 0. \tag{2.10}$$

Equation (2.9) is simply a restatement of the KdV equation given in (1.1), while (2.10) reduces to a similar equation where the sign of the linear phase speed is reversed. Thus, the leading-order wave field requires the solution of two independent KdV equations on the interval $[0, L]$, where the initial condition for each KdV equation is given by $\eta_0/2$. To leading order, the displacement field can, therefore, be obtained by solving both equations on the periodic interval $[0, L]$ and subsequently summing the separate solutions at every instant in time. However, consideration of the boundary conditions $u_i(0,t) = u_i(L,t) = 0$, together with the expressions for the leading-order velocity field

$$u_1(x,t) = \frac{1}{h_1}\mathscr{N}_t, \quad u_2(x,t) = -\frac{1}{h_2}\mathscr{N}_t, \tag{2.11}$$

shows that the complete solution must satisfy $\mathscr{N}(0,t) = \mathscr{N}(L,t) = 0$. This immediately suggests the use of an even half-range expansion of the displacement field: that is, we consider the solution of the two KdV equations in the extended domain $[0, 2L]$ with symmetry about the position $x = L$. Now, it is readily apparent that the solution $g(s,\tau)$ in $[0, L]$ is equivalent to the solution $f(r,\tau)$ in $[L, 2L]$ folded about the line $x = L$. Furthermore, since the initial condition (the displacement η_0) is split equally between $f(r,0)$ and $g(s,0)$, we can realize the solution $\eta^{(1)} = f(r,\tau) + g(s,\tau)$ by solving only the single KdV equation for the field $f(r,\tau)$ in the interval $[0, 2L]$ using periodic boundary conditions and with initial condition $\eta_0/2$ as shown in figure 1. The desired field in the physical domain $[0, L]$ is obtained subsequently by folding the solution field for $f(r,\tau)$ in $[L, 2L]$ about $x = L$ (i.e. using $g(x,t) = f(2L - x, t)$) to obtain the desired bi-directional evolution.

The second-order contribution $\mathscr{N}^{(2)}$, which contains the leading estimate of the interaction between waves propagating in opposite directions, can be calculated from the remaining (non-secular) term on the right-hand side of (2.6). Evaluating the particular solution for $\eta^{(2)}$ in terms of the separate d'Alembert functions yields

$$\eta_p^{(2)} = \frac{\partial \mathscr{N}_p}{\partial X} = \frac{\partial \mathscr{N}_p^{(2)}}{\partial r} + \frac{\partial \mathscr{N}_p^{(2)}}{\partial s} = \frac{1}{4}\frac{h_1 - h_2}{h_1 h_2}\{2fg + f_r G + g_s F\}. \tag{2.12}$$

Now, using the fact that $g(x,t) = f(2L - x, t)$ in $0 \leqslant x \leqslant L$, and the definitions in (2.8), the interaction contribution can be re-written as

$$\eta_p^{(2)} = \frac{1}{4}\frac{h_1 - h_2}{h_1 h_2}\left\{2f(x,t)f(2L - x,t) + \frac{\partial f(x,t)}{\partial x}\int_{2L}^{2L-x} f(2L - x', t)\,\mathrm{d}x' + \frac{\partial f(2L - x, t)}{\partial x}\int_{x=0}^{x} f(x', t)\,\mathrm{d}x'\right\}, \quad 0 \leqslant x \leqslant L. \tag{2.13}$$

This interaction correction applies at any instant in time and can be computed

after integration of the single KdV equation for the function $f(r,\tau)$ in $[0,2L]$ has been accomplished. There is a further component in the complete solution for $\eta^{(2)}$ involving nonlinear interactions between $\eta^{(1)}$ and $\eta_p^{(2)}$, but we choose to neglect that contribution. Our goal is to propose a rapid calculation tool for weakly nonlinear evolution in closed basins, and this additional component would require integration of further PDEs involving the non-local term $\eta_p^{(2)}$.

An approximate solution for the long-wave evolution in a closed basin of length L can, therefore, be obtained by the integration of a single KdV equation on the extended interval $[0,2L]$. The leading-order solution is obtained by folding the computed KdV field about the symmetry line $x = L$. The second-order correction can be added by including the sum of the factors given in (2.13), which involves the computation of the two quadratures. An implicit advantage of the (natural) even extension of the solution domain is that both the initial condition and any bottom topography will be continuous functions. Hence, any artificial introduction of high-wavenumber behaviour in the spatial representation of the wave field will be ameliorated. Of course, discontinuities of spatial derivatives of the initial condition and/or the bottom topography may still enter, but this is of comparatively minor significance in any numerical simulation of the KdV equation.

2.2. *Numerical method*

The physical bi-directional domain $[0,L]$ is first extended to form the uni-directional domain $[0,2L]$ and discretized into equal intervals with periodic boundary conditions at $x = 0, 2L$. The initial interface displacement $\eta_0(x)$ in the physical bi-directional domain $[0,L]$ is then divided and apportioned equally to form the initial conditions $f(x,0)$ and $g(x,0)$. Recalling that $g(x,t) = f(2L-x,t)$, we have

$$f(x,0) = f(2L-x,0) = \tfrac{1}{2}\eta_0(x), \quad 0 \leqslant x \leqslant L. \tag{2.14}$$

To solve the KdV equation, from which the leading-order wave field is obtained, we use a pseudo-spectral method (Canuto *et al.* 1988).

Since we later make direct comparisons of the evolution predicted by the model (2.8) with laboratory experiments, it is important to include in the model dissipative effects arising from laminar boundary layers along the surface of the tank. To this end we employ an extended KdV equation (cf. Keulegan 1948; Miles 1976) applicable to an infinitely wide tank with rigid upper and lower surfaces, the form of which is well suited to the psuedo-spectral method employed here:

$$\begin{aligned} f_t + \alpha f f_x + \beta f_{xxx} &= \frac{1}{2}\sqrt{\frac{\nu c_0}{2}}\frac{h_1+h_2}{h_1 h_2}\frac{1}{2\pi}\int_{-\infty}^{\infty} |k|^{1/2}(-1+\mathrm{isgn}\,k)\hat{f}(k,t)\,\mathrm{e}^{ikx}\,\mathrm{d}k \\ &= \frac{1}{2}\sqrt{\frac{\nu c_0}{2}}\frac{h_1+h_2}{h_1 h_2}\mathscr{F}^{-1}\{|k|^{1/2}(-1+\mathrm{isgn}\,k)\hat{f}(k,t)\}, \end{aligned} \tag{2.15}$$

where ν is the kinematic viscosity.

The second-order correction (2.13) is computed at whatever time is of interest. Since the correction is evaluated after the integration of the KdV equation is completed, it in no way influences the spectral accuracy of the numerical integration of the KdV equation. The spatial derivatives required by the correction are calculated using the same spectral method and the integrals are calculated using the trapezoidal rule. A time series of the value of this second-order correction at a point can be generated by evaluating the integral at each timestep, such as for figure 7, but this is not necessary.

The model has been developed to describe the nonlinear evolution of basin-

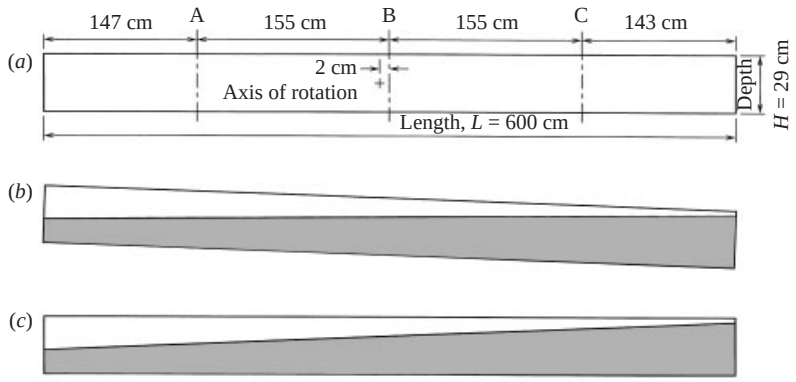

FIGURE 2. (*a*) Schematic diagram of the experimental set-up. The ultrasonic wavegauges were located at the positions marked A, B and C. (*b*, *c*) The tank and the density structure immediately before and after an experiment commences: (*b*) initially tilted tank, (*c*) initial condition with the tank horizontal and interface inclined.

scale waves in a laboratory experiment. We therefore keep the variables in their original physical dimensions. For modelling the laboratory experiments in a 6 m tilting tube, the reflected domain was 12 m long and was discretized into 512 intervals of $\Delta x = 0.023$ m and the timestep was $\Delta t = 0.001$ s, although substantially coarser grid spacings and timesteps are possible for weakly nonlinear simulations.

3. Comparison with laboratory results

3.1. *Laboratory experiments*

The laboratory experiments described below were part of a wider study of the degeneration of large-scale interfacial waves in lakes by Horn *et al.* (2001) and the interested reader is referred to that work for more detail. The laboratory experiments were conducted in a clear acrylic tank 600 cm long, 29 cm deep and 30 cm wide. The tank could rotate about a horizontal axis approximately through its centre so that the interface could be initially tilted. The experimental set-up is shown in figure 2. The tank was filled with a two-layer stratification ($0.2 < h_2/H < 0.3$), the upper layer being fresh and the lower layer saline ($\Delta\rho \approx 20\,\mathrm{kg\,m^{-3}}$) and the interface thickness was less than 1 cm. Before starting the experiment the tank was slowly rotated through a small angle ($\theta = 0.25^\circ$–1.5°) to its initial position.

The experiment began at $t = 0$ when the tank was suddenly returned to a horizontal position so that the interface was then inclined at the original angle of tilt, as shown in figure 2. The resulting flow was recorded on video and the interface displacement measured by ultra-sonic wavegauges (Michallet & Barthélemy 1997). For experiment A, the depth of the lower layer was 5.8 cm ($h/H = 0.2$) and the initial angle of tilt was 0.5°. To allow a range of initial amplitudes to be considered, we also present the results from a series of experiments (B1–4) in which the lower layer was 8.5 cm ($h/H = 0.3$) and the angle of tilt was increased from 0.25° to 1.0°. Since this second series of experiments was conducted without re-filling the tank, the interface gradually thickened during the series from approximately 1 cm to 2 cm.

When the experiment began at $t = 0$ with the interface suddenly inclined, the baroclinic pressure gradient drove a flow from right to left below the interface and from left to right above it. In experiment A the interface was observed to initially oscillate about its horizontal position, as predicted by linear theory (e.g. Spigel &

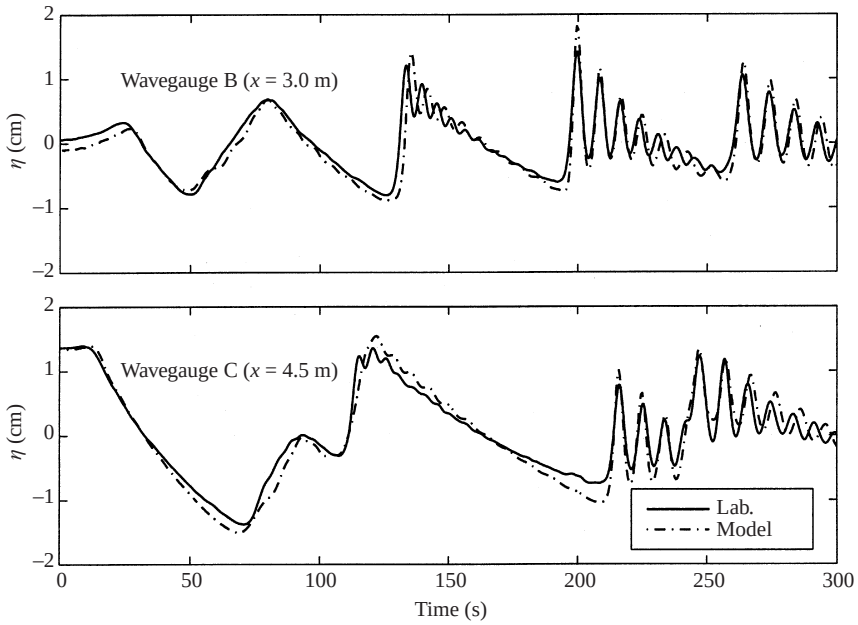

FIGURE 3. Comparison of simulated and observed interface displacements. Time series of interfacial displacements at horizontal positions corresponding to wavegauges B ($x = 3.0$ m) and C ($x = 4.5$ m). For this experiment (A) $h = 5.8$ cm, $H = 29$ cm, $\theta = 0.5°$ and $\Delta\rho = 20\,\mathrm{kg\,m^{-3}}$.

Imberger 1980). However, at about $t = 90$ s the basin-scale standing wave developed an asymmetry and its front face gradually steepened. By $t = 150$ s a train of solitons was seen to emerge. We will refer to these waves initially as solitons, but will show in § 4.2 that they include dispersive oscillatory waves as well as KdV solitons. These waves were reflected from the endwalls and continued to propagate back and forth through the tank. After each reflection the waves passed through one another but appeared unaffected by the interaction. They were gradually damped, but were still visible on the wavegauge outputs after 1000 s when the instrument and video records were terminated. The evolving wave field can be seen by examining the time series of interface displacements recorded by the ultrasonic wavegauges as shown in figure 3. Wavegauge B was located near the centre of the tank ($x \approx 3.0$ m) and wavegauge C at the 3/4 position ($x \approx 4.5$ m).

The wavegauge outputs for experiments B1–B4, with increasing angle of tilt, are shown in figure 4. In experiment B1 the amplitude of the initial basin-scale wave was very small and the interface oscillated as a standing wave (without evolving into solitons) until the motion was eventually damped by viscous effects. However, when the amplitude of the initial wave was increased (by increasing the angle of tilt), the initial basin-scale wave was observed to steepen more rapidly and the number and amplitude of solitons increased.

3.2. *Numerical simulations*

The model described in § 2.2 was used to simulate laboratory experiment A. Following the method described in § 2.1, half the initial interface displacement over the 6 m length of the tank was reflected about $x = 6$ m onto the extended discretized 12 m domain, as shown in figure 5. The model was then run for 600 s of real time and the physical interfacial displacements recovered by folding the 12 m computational domain about

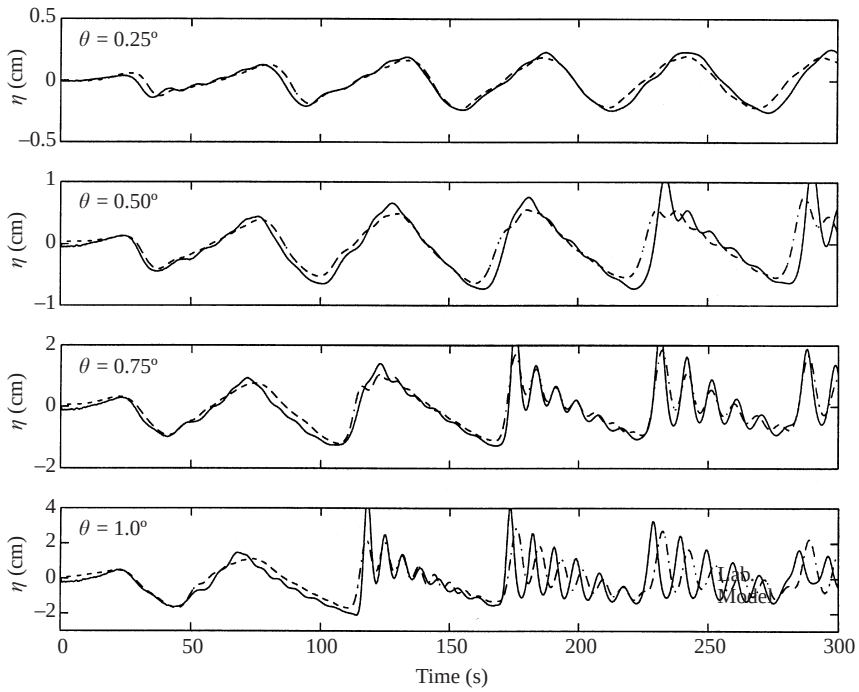

FIGURE 4. Comparison of simulated and observed interface displacements. Time series of interface displacements at wavegauge B predicted by the model (—) and from the laboratory experiments B1–B4 (- · -). For these experiments $h = 8.5\,\text{cm}$, $H = 29\,\text{cm}$, $0.25° < \theta < 1.0°$ and $\Delta\rho = 20\,\text{kg m}^{-3}$.

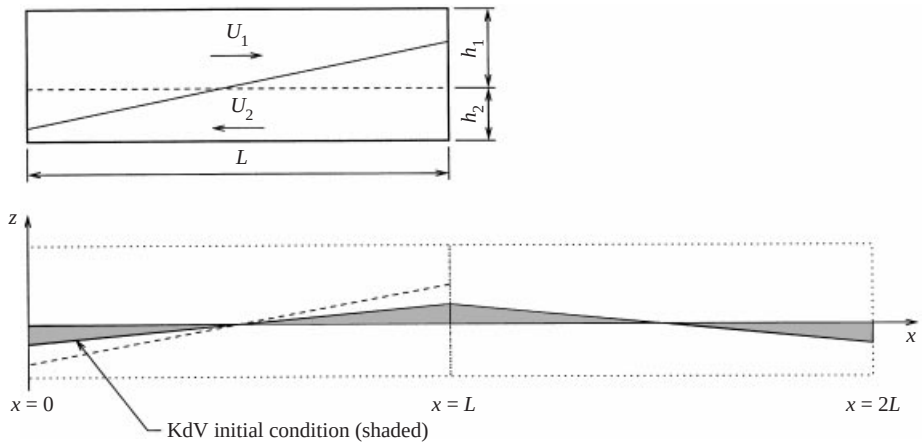

FIGURE 5. Schematic diagram of initial condition for the model. The displacement due to the tilted interface is partitioned equally into leftward and rightward propagating parts by taking half the laboratory initial condition and reflecting it about $x = L$ in the extended reflected domain.

$x = 6\,\text{m}$. The first-order KdV solution and the second-order interaction term were calculated separately and then summed.

The solution from the model, consisting of the sum of the first-order KdV solution and the second-order interaction term, is shown in figure 6, in which the simulated interface position is plotted at intervals of $T_i/4$, where T_i is the period of the basin-

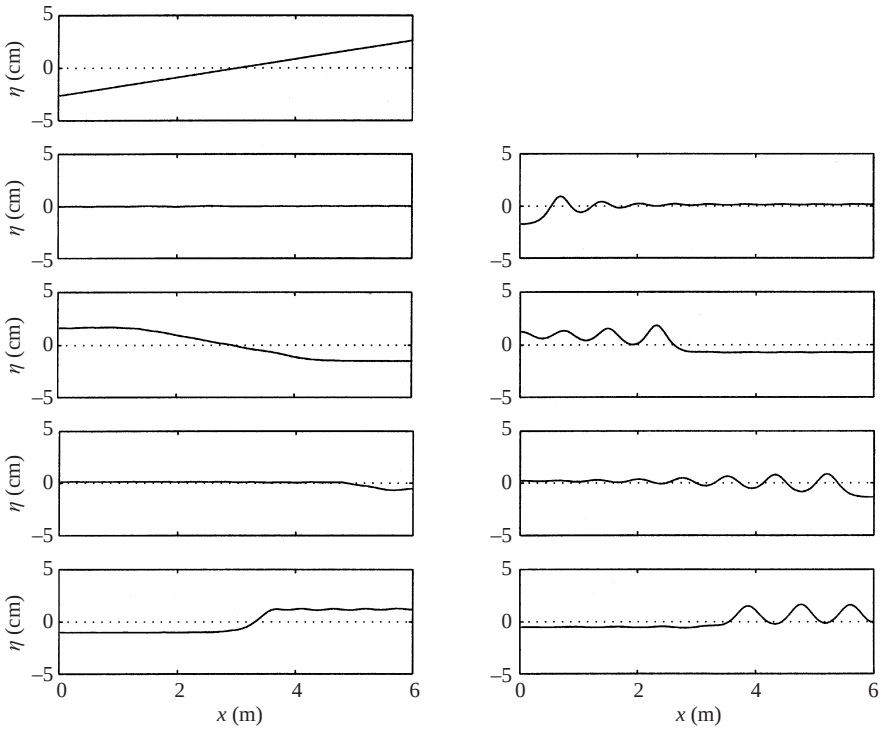

FIGURE 6. Results of a model simulation: interface displacements plotted at intervals of $T_i/4$. For this experiment (A) $h = 5.8$ cm, $H = 29$ cm, $\theta = 0.5^\circ$ and $\Delta\rho = 20\,\mathrm{kg\,m^{-3}}$.

scale linear internal wave. The model reproduces the steepening of the basin-scale wave and the evolution of solitons, closely matching the video record of the laboratory experiment.

Figure 3 shows that the interface displacements simulated by the model are close to those recorded by the ultrasonic wavegauges. The model slightly over-predicts the amplitude of the emerging solitons, but captures the timing and phase of their evolution very well. After 300 s the phase error of the leading three solitons measured at wavegauge 2 was less than 1 s (10 cm) although the amplitude error was more significant (0.2 cm = 13%). The phase errors of the smaller solitons were greater, with the laboratory wave packet appearing more compact. Although figure 3 only shows the first 300 s of data, after 600 s the model was still closely reproducing the laboratory signal. At 600 s, the phase error of the leading soliton measured at wavegauge B was 2 s (19 cm) and the amplitude error was 0.05 cm (15%).

In making any detailed comparison between the model simulation and the experimental results we should note that the model includes several simplifying assumptions and that the experimental data contain some uncertainties, all of which contribute to the observed differences. For example, some of the phase errors could easily be attributed to the continuous stratification in the experiments which is being modelled by a two-layer system (Helfrich & Melville 1986). Furthermore, to model the actual continuous stratification of the experiments as a two-layer system, an equivalent interface depth is calculated. Apart from the fact that the linear long-wave speed on a finite thickness interface is less than that of the true two-layer case, the wave speed is also quite sensitive to the interface depth. An error in the assumed interface

depth (based on the measured continuous density profile) of $\pm 5\%$ of the depth of the lower layer (± 0.3 cm over 5.8 cm) would lead to a phase difference of ± 6 s over 300 s. Other possible sources of small errors are the measurements of initial angle of tilt and the density difference. The model also neglects viscous losses at the endwalls and sidewalls of the tank and at the interface, an omission that might contribute to the over-prediction of the wave amplitudes. These additional terms could each be added to the dissipative term if the model was to be used for a quantitative analysis of the laboratory experiments.

To further test its performance, the model was used to simulate a sequence of laboratory experiments with increasing nonlinearity. Figure 4 compares the predicted and recorded interface displacements. Considering that the simulations are based on a two-layer weakly nonlinear approximation, the model reproduces well the laboratory data over the considerable range of dynamic behaviours shown in figure 4, although it does generally over-predict the amplitude of the emerging solitons. We suggest that an explanation for these errors in amplitude is a combination of the simple boundary dissipation model used and the assumption of weak nonlinearity. The comparisons in figure 4 show that the model does less well in simulating experiments with strong nonlinearity, that is for experiments with larger angles of tilt. The Boussinesq and KdV equations require that the nonlinearity is weak ($\epsilon \ll 1$) and Koop & Butler (1981) showed that the KdV equation was valid for amplitudes as large as $\epsilon \approx 0.2$. Including higher-order terms or cubic nonlinearity would be expected to improve the quantitative agreement with the laboratory experiments. However, our purpose in this paper is to propose a tool for use in understanding the qualitative evolution of the internal wave field in lakes.

4. Discussion

4.1. *Wave–wave interactions*

A feature of the laboratory experiments presented in § 3.1, and of the internal wave field in many closed basins, is wave–wave interactions. In two-dimensional closed basins, these interactions fall into two categories: one in which both waves are propagating in the same direction, and the other in which the waves are propagating in opposite directions. In the case of the degeneration of basin-scale waves in closed basins, the evolution of the internal wave field necessarily involves the continual interaction of waves propagating in both directions. The reflection of a wave from a vertical endwall is approximately equivalent to its interaction with an identical wave travelling in the opposite direction and so falls into the second category.

The first class of interaction, in which waves overtake one another while travelling in the same direction, has been described as the *strong* interaction (e.g. Miles 1977; Weidman & Maxworthy 1978). In this case both waves possess the same linear phase speed and the interaction occurs on a long timescale determined by the differences in wave amplitudes (i.e. differences in the nonlinear corrections to the phase speed). This type of interaction is implicitly included in the two KdV equations (2.9) and (2.10) and has been studied analytically (e.g. Lax 1968), numerically (e.g. Fornberg & Whitham 1978) and in the laboratory (e.g. Weidman & Maxworthy 1978). An important property of KdV solitary waves is that following such a strong interaction they preserve their form. Although each wave experiences a phase shift (the larger, faster wave has a forward phase shift and the slower, smaller wave has a backward

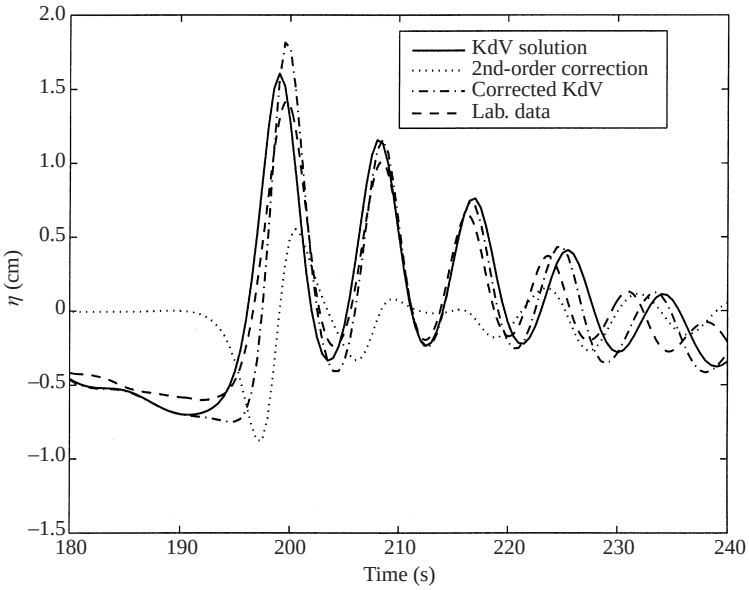

FIGURE 7. Effect of the second-order correction term. Comparisons of the solutions given by the independent KdV equations (2.8), the solution with the second-order correction (2.13), and the experimental data. The plots are for time series of interfacial displacements at wavegauge B ($x = 3.0$ m). The experimental parameters were the same as for figure 6.

shift), in an inviscid system they maintain their shape and amplitude and there is no loss of energy.

The second type of interaction, between waves travelling in opposite directions, occurs on a relatively fast (actually, a much faster) timescale associated with the linear phase speed and the respective wavelengths and has been described as the *weak* interaction. The effects of the interaction are of higher order than the KdV equation and a first approximation to the solution can be obtained by linearly superposing the KdV solutions along each characteristic (Miles 1977). This approximation is equivalent to the leading-order solution described by (2.8) and is plotted in figure 7 as the KdV solution. The second-order solution described in § 2.1 includes the wave–wave interactions as an asymptotically smaller term given by (2.13). This is clearly an approximation to the Boussinesq equation (2.1), which makes no approximation regarding the wave–wave interaction of either class beyond the weakly nonlinear assumption underlying the derivation of the equation from first principles.

Figure 7 plots the magnitude of the first-order approximation (2.8), the second-order correction (2.13), and the subsequently corrected approximation given by the sum of these two terms, together with the laboratory data. The first-order approximation, formed by sum of the independent KdV equations, provides a good approximation of the laboratory observations, although there is a phase error over the length of the wave packet. The two leading KdV waves are ahead of the corresponding laboratory waves, but the subsequent KdV waves lag behind the laboratory waves, so that the KdV wave packet is more dispersed than the observed laboratory wave packet. The main effect of the second-order correction is to introduce a phase shift to each wave, backwards in the case of the two leading waves and forwards for the trailing waves, improving the match between the phase of the waves in the model and the

laboratory data. The inclusion of the second-order correction does, however, increase the amplitude error of the leading soliton.

The most obvious wave–wave interactions observed in the laboratory experiments occur during the reflection of the wave packet from the endwall of the tank when the wave packet passes through itself so that each wave interacts with each of the other waves in the same packet while travelling in the opposite direction. The interaction of two solitary waves propagating in opposite directions has been investigated in analytical studies (Byatt-Smith 1971; Gear & Grimshaw 1984), laboratory experiments (Maxworthy 1976; Renouard, Seabra-Santos & Temperville 1985) and numerical simulations (Mirie & Su 1982; Fenton & Rienecker 1982; Cooker, Weidman & Bale 1997). These studies show that the collision of two solitary waves results in a maximum amplitude exceeding the sum of the interacting waves and that each wave emerges with a negative phase shift. None of these studies, however, predict the positive phase shift observed in our laboratory experiments and the numerical simulations.

The studies cited above focused only on the interaction of solitons and the bottom panel of figure 3 shows that the packet of solitons is interacting with some large-scale wave that moves the entire interface up and down. The source and role of this large-scale wave is examined in the following section but we note here that its interaction with the soliton packet appears to be approximated by the proposed model (since the positive phase shift observed in the laboratory data is reproduced in the model).

4.2. *Decomposition of the internal wave field*

That the KdV equation captures so much of the dynamics of the degeneration of the basin-scale initial condition confirms that nonlinear steepening and dispersive effects dominate this process. We now investigate the composition of the evolving internal wave field in terms of the known behaviour of some simple solutions to the KdV equation. It is, of course, true that the wave field described by the KdV model applied here to the extended-folded closed domain is properly given by consideration of the periodic inverse scattering transform (e.g. Osborne *et al.* 1998). However, we find that it is useful for conceptual purposes to think of the wave field as being composed of two separate parts emanating from the two different displacement volumes that co-exist, but are spatially separated, during any realistic distortion of the interface in a closed basin.

If we initially consider the initial condition $\eta_0(x)$ for waves travelling along only one of the characteristics and described by (1.1) when the nonlinear coefficient α is positive, it can be shown (e.g. Drazin & Johnson 1989) that for solutions on the infinite line:

(*a*) When the net volume of the initial condition is positive ($\int \eta_0 \, \mathrm{d}x > 0$), it evolves into at least one soliton and a tail of dispersive oscillatory waves. The number of solitons can be determined from the initial condition by employing the inverse scattering transform.

(*b*) When $\eta_0(x) \leqslant 0$ for all x, no solitons emerge and the solution consists of a negative leading wave, referred to as a rarefaction, and a dispersive train of oscillatory waves.

The tilted interface that formed the initial condition for the laboratory experiments consisted of both positive ($\eta_0(x) > 0$) and negative ($\eta_0(x) < 0$) displacement of the interface with a net volume $\int \eta_0 \, \mathrm{d}x = 0$ by conservation of volume in a closed basin. For the KdV model simulations figure 8 shows the separate evolution of the positive and negative volumes that make up the tilted interface, and figure 3 shows the evolution of the complete initial condition. It is the superposition and nonlinear

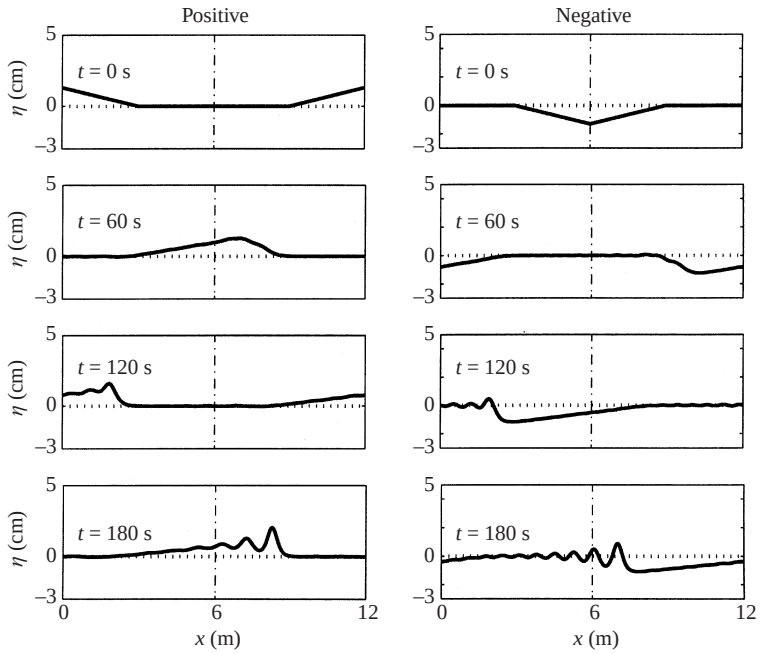

FIGURE 8. Evolution of positive and negative initial volumes. An initial condition of the form of a tilted interface can be decomposed into a positive and a negative initial displacement. The positive initial condition will evolve into at least one soliton. For the case of a thin lower layer the solitons are waves of elevation. The negative initial condition evolves into a negative dispersive wave, referred to as a rarefaction, and a train of dispersive oscillatory waves. The dispersive oscillatory waves are initially similar in appearance to the solitons. The wave field that evolves from the case of the tilted interface is a result of the nonlinear interaction of all of these waves.

interaction of these different waves (emerging from the positive and negative volumes) that produces the observed interface displacements. For the usual case of a semi-infinite domain, it can be shown (e.g. Hammack & Segur 1974; Horn *et al.* 2000) that for such simple initial conditions, the number and amplitude of emerging solitons is determined by the positive volume only, and that the long-term behaviour of the emerging solitons is independent of the presence of the negative volume. Similarly, the negative volume evolves into a leading rarefaction and a dispersive train of oscillatory waves that, in the long term, are relatively unaffected by the presence of the positive volume. If the positive volume is initially to the left of the negative volume (for the case of the rightward characteristic), the evolving solitons, having a greater phase speed, first pass through the oscillatory waves and the trough of the negative wave. The interaction between the solitons and dispersive waves affects the short-term evolution of the wave field by changing the depth of the interface on which the waves propagate and by introducing phase shifts to the solitons. However, in the long term the waves separate in space into a packet of solitons and a packet of dispersive waves (consisting of the leading negative wave and the oscillatory tail). The situation in a closed basin such as the laboratory tank appears more complicated because these different components are unable to separate in space. The waves continue to pass through one another as they are reflected from the endwalls and these repeated interactions are thought to be the cause of the positive phase shifts observed in the laboratory experiments. Nonetheless, an initial condition such as the tilted interface considered here will evolve into an internal wave field that can be described in terms

of three components, each of which behaves differently. The KdV equation has been shown to closely predict the evolution of all these waves in the case of surface waves Hammack & Segur (1978), except the possibility of high-wavenumber oscillatory waves forming envelope solitons or becoming unstable. Since these effects occur on relatively long timescales compared with the effects of interest here, this shortcoming is considered acceptable.

The solitons emerge from the initial positive volume after a time $T_s \sim L/\alpha\eta_0$ (Horn *et al.* 2001), at which time the leading wave has an amplitude $a \sim \eta_0$ and a characteristic wavelength

$$\lambda = \left(\frac{12}{a}\frac{\beta}{\alpha}\right)^{1/2}, \tag{4.1}$$

where α and β are the coefficients of the KdV equation (1.1). These waves are much shorter than the basin-scale initial condition from which they emerged. In a closed basin with sloping ends, such as a lake, these solitons would shoal at the first boundary. Although the shoaling of these waves is a function of the wave amplitude (and hence slope) and the boundary slope, for typical lake slopes solitary waves might dissipate upto 70% of their energy in a single reflection (Michallet & Ivey 1999; Helfrich 1992).

The negative wave behaves quite differently. The front slope of the wave decreases with time, the wavelength increases as $O(t^{1/3})$ and the amplitude decreases as $O(t^{-1/3})$ (Ablowitz & Segur 1977). This rarefaction initially has a wavelength that is comparable with half the basin length and slowly grows in length. Unlike the much shorter solitons, this wave would be reflected from typical lake boundaries, remaining in the lake for a considerable time after the wind event that generated it.

The rarefaction is followed by a train of dispersive oscillatory waves. The amplitude of the leading oscillatory waves is $\sim \eta_0$ and their wavelength is comparable with that of the solitons given by (4.1). However, the amplitude and wavelength of the oscillatory waves decreases towards the back of the train and their amplitude decays as $O(t^{-1/3})$. The leading waves in the packet have a phase speed approaching, but less than, the linear long-wave speed and the phase speed of the following waves decreases towards the back of the train, so the packet disperses with time. These oscillatory waves emerge from the initial negative volume at approximately the same time as, and with similar characteristics to, the solitons that emerge from the initial positive volume. Furthermore, in simulations of the laboratory experiments the leading oscillatory waves first appear in the same region in space and have a similar phase speed as the solitons and appear to remain in phase with them, initially giving the appearance of a larger packet of solitons. However, in time the oscillatory waves decay in amplitude and become separated from the true solitons. Since they are also relatively short waves compared with typical lake slopes (although still long waves), they will break at the first sloping boundary they encounter.

An interesting question that arises from this description is whether, once the solitons and oscillatory waves have shoaled at the boundaries, the residual wave steepens again, starting the cycle once more. The only waves that will steepen to form more solitons are positive waves (usually waves of depression in lakes). Since the rarefaction is a negative wave it will never steepen to generate solitons. The shoaling of solitons at sloping boundaries does not dissipate all of the incident wave energy and Michallet & Ivey (1999) observed reflected small-amplitude long waves. These long waves would steepen, although whether they degenerate into a packet of solitons would depend on the competition between damping and steepening.

We suggest that in many lakes the conceptual model of a linear internal standing

wave, or seiche, is inappropriate and should be replaced by a weakly nonlinear model such as the one based on the KdV equation and presented here. The action of the wind blowing over the surface of a lake is to generate a depression of the thermocline at the leeward shore and an elevation of the thermocline at the windward shore. In the absence of rotation, these displacements of the thermocline form the initial positive and negative volumes from which evolve the three components described above. Note that in most lakes the thermocline is above the mid-depth position so that a depression of the thermocline represents a positive initial volume. Conservation of volume requires that any depression of the thermocline must be accompanied by an equal elevation of the thermocline, so all three components will always emerge from any displacement of the thermocline (although not from the same location) unless they are damped by boundary dissipation. In many cases, such as a tilted thermocline, the potential energy of the initial condition is equally divided between the positive and negative volumes, so that the long rarefaction should be as important to the internal wave dynamics as the more commonly described internal solitons and surge that evolve from the downwelled, positive volume. In many lakes, the recorded isotherm displacements with periods close to that of the linear internal standing wave could be due to a propagating rarefaction, rather than a linear standing wave. A rarefaction would take the form of an asymmetric large-scale wave of elevation, but unless the true background stratification is known, this could be misinterpreted as a basin-scale oscillation. During the early stages of steepening the combination of the propagating rarefaction in combination with the steepening wave of depression would appear similar to a basin-scale standing wave. Equally important, the groups of solitons and oscillatory waves could be misinterpreted from spectral analysis as a spectrum of internal waves, rather than a set of groups of high-frequency waves.

5. Conclusions

We have developed a simple KdV-type model for describing the weakly nonlinear evolution of long interfacial waves in a closed basin. The solution method is based on an approximation of the Boussinesq equation and consists of the sum of the solutions of two independent KdV equations and a second-order interaction term. The solution of the two independent KdV equations is obtained by first taking half the initial condition (on $[0, L]$) and reflecting it onto an extended uni-directional domain $[0, 2L]$ (with periodic boundary conditions), then integrating a single KdV equation on the extended domain. The solution is then folded about $x = L$ to obtain the bi-directional wave field.

The model was validated against a series of laboratory experiments in which an initial basin-scale wave steepened and evolved into packets of shorter waves and some residual basin-scale waves. Despite some simplifying assumptions (weakly nonlinear; two-layer stratification; no mixing; simple boundary loss model) the model reproduced the observed interface displacements qualitatively very well. A comparison of the leading-order KdV solution and the second-order correction (that includes the approximate interaction term) shows that the main effect of the second-order correction is to introduce a phase shift to each wave, improving the phase match between the model and the laboratory data, although increasing the amplitude error of the leading soliton.

We have shown that an initial tilted interface can be decomposed into a positive and a negative volume (in terms of the KdV model), and that the evolving internal wave field can then be qualitatively described in terms of the nonlinear interaction of waves

that emerge from these positive and negative initial conditions. The resulting wave field consists of three components: a train of solitons, a dispersive long wave referred to as a rarefaction and a train of dispersive oscillatory waves. Any displacement of the interface in a closed basin can similarly be decomposed into positive and negative initial conditions for the KdV equation and the resulting wave field will always consist of these three components (provided that the damping timescale is slower than the steepening timescale).

The generation of solitons and dispersive oscillatory waves from any initial condition has important implications for the energy cascade in lakes. These relatively short waves shoal and break at the shallow-sloping boundaries in lakes, dissipating much of their energy and contributing to the turbulence in the benthic boundary layer and reflecting some energy as smaller-amplitude long waves. Conversely, the long rarefaction is reflected from the sloping boundaries and continues to propagate back and forth across the lake, gradually growing in length and decaying in amplitude. We suggest that the basin-scale waves observed in many lakes are not true linear standing waves, but a combination of propagating rarefactions (taking the form of a waves of elevation) and long waves of depression.

The model described here is based on the standard KdV equation for a two-layer stratification, modified only to account for laminar boundary layer losses. We are currently adapting the model to include effects such as variable topography, wind forcing and the breaking of waves at sloping boundaries.

The authors are grateful to Kraig Winters for his assistance in implementing the numerical method. This research was supported by the Centre for Environmental Fluid Dynamics and the Australian Research Council and was completed while D. A. H. was a recipient of an Australian Postgraduate Award and a Samaha Research Scholarship. This paper is Centre for Water Research reference ED 1436DH. L. G. R. acknowledges the assistance of the Gledden Trust in providing support via a Gledden Senior Visiting Fellowship at The University of Western Australia, and other partial support provided by the Office of Naval Research under Grant N00014-95-0041.

REFERENCES

Ablowitz, M. J. & Segur, H. 1977 Asymptotic solutions of the Korteweg–de Vries equation. *Stud. Appl. Maths* **57**, 13–44.

Byatt-Smith, J. G. B. 1971 An integral equation for unsteady surface waves and a comment on the Boussinesq equation. *J. Fluid Mech.* **49**, 625–633.

Canuto, C., Hussaini, M. Y., Quarteroni, A. & Zang, T. A. 1988 *Spectral Methods in Fluid Dynamics.* Springer.

Cooker, M. J., Weidman, P. D. & Bale, D. S. 1997 Reflection of a high-amplitude solitary wave at a vertical wall. *J. Fluid Mech.* **342**, 141–158.

Djordjevic, V. D. & Redekopp, L. G. 1978 The fission and disintegration of internal solitary waves moving over two-dimensional topography. *J. Phys. Oceanogr.* **8**, 1016–1024.

Drazin, P. G. & Johnson, R. S. 1989 *Solitons: An Introduction.* Cambridge University Press.

Farmer, D. M. 1978 Observations of long nonlinear internal waves in a lake. *J. Phys. Oceanogr.* **8**, 63–73.

Fenton, J. D. & Rienecker, M. M. 1982 A Fourier method for solving nonlinear water-wave problems: application to solitary-wave interactions. *J. Fluid Mech.* **118**, 411–443.

Fornberg, B. & Whitham, G. B. 1978 A numerical and theoretical study of certain nonlinear wave phenomena. *Phil. Trans. R. Soc. Lond.* A **289**, 373–404.

Gear, J. A. & Grimshaw, R. 1984 Weak and strong interactions between internal solitary waves. *Stud. Appl. Maths* **70**, 235–258.

Hammack, J. L. & Segur, H. 1974 The Korteweg–de Vries equation and water waves. Part 2. Comparison with experiments. *J. Fluid Mech.* **65**, 289–314.

Hammack, J. L. & Segur, H. 1978 The Korteweg–de Vries equation and water waves. Part 3. Oscillatory waves. *J. Fluid Mech.* **84**, 337–358.

Heaps, N. S. & Ramsbottom, A. E. 1966 Wind effects on the water in a narrow two-layered lake. *Phil. Trans. R. Soc. Lond.* A **259**, 391–430.

Helfrich, K. R. 1992 Internal solitary wave breaking and run-up on a uniform slope. *J. Fluid Mech.* **243**, 133–154.

Helfrich, K. R. & Melville, W. K. 1986 On long nonlinear waves over slope-shelf topography. *J. Fluid Mech.* **167**, 285–308.

Helfrich, K. R., Melville, W. K. & Miles, J. W. 1984 On interfacial solitary waves over slowly varying topography. *J. Fluid Mech.* **149**, 305–317.

Horn, D. A., Imberger, J. & Ivey, G. N. 2001 The degeneration of large-scale interfacial gravity waves in lakes. *J. Fluid Mech.* **434**, 181–207.

Horn, D. A., Redekopp, L. G., Imberger, J. & Ivey, G. N. 2000 Internal wave evolution in a space-time varying field. *J. Field Mech.* **424**, 279–301.

Hunkins, K. & Fliegel, M. 1973 Internal undular surges in Seneca Lake: a natural occurrence of solitons. *J. Geophys. Res.* **78**, 539–548.

Hutter, K., Bauer, G., Wang, Y. & Güting, P. 1998 Forced motion response in enclosed lakes. In *Physical Processes in Lakes and Oceans* (ed. J. Imberger). AGU.

Imberger, J. 1998 Flux paths in a stratified lake: a review. In *Physical Processes in Lakes and Oceans* (ed. J. Imberger). AGU.

Keulegan, G. H. 1948 Gradual damping of solitary waves. *J. Res. Natl Bur. Stand.* **40**, 487–498.

Koop, C. G. & Butler, G. 1981 An investigation of internal solitary waves in a two-fluid system. *J. Fluid Mech.* **112**, 225–251.

Lax, P. D. 1968 Integrals of nonlinear equations of evolution and solitary waves. *Commun. Pure Appl. Maths* **21**, 467–490.

Lee, C.-Y. & Beardsley, R. C. 1974 The generation of long nonlinear internal waves in a weakly stratified shear flow. *J. Geophys. Res.* **79**, 453–462.

Maslowe, S. A. & Redekopp, L. G. 1980 Long nonlinear waves in stratified shear slows. *J. Fluid Mech.* **101**, 321–348.

Maxworthy, T. 1976 Experiments on collisions between solitary waves. *J. Fluid Mech.* **76**, 177–185.

Michallet, H. & Barthélemy, E. 1997 Ultrasonic probes and data processing to study interfacial solitary waves. *Exps. Fluids* **22**, 380–386.

Michallet, H. & Ivey, G. N. 1999 Experiments on mixing due to internal solitary waves breaking on uniform slopes. *J. Geophys. Res.* **104**, 13467–13478.

Miles, J. W. 1976 Damping of weakly nonlinear shallow-water waves. *J. Fluid Mech.* **76**, 251–257.

Miles, J. W. 1977 Obliquely interacting solitary waves. *J. Fluid Mech.* **79**, 157–169.

Miles, J. W. 1981 The Korteweg–de Vries equation: a historical essay. *J. Fluid Mech.* **106**, 131–147.

Mirie, R. M. & Su, C. H. 1982 Collisions between two solitary waves. Part 2. A numerical study. *J. Fluid Mech.* **115**, 475–492.

Mortimer, C. H. 1952 Water movements in lakes during summer stratification; evidence from the distribution of temperature in Windermere. *Phil. Trans. R. Soc. Lond.* B **236**, 355–404.

New, A. L. & Pingree, R. D. 2000 An intercomparison of internal solitary waves in the Bay of Biscay and resulting from Korteweg–de Vries-type theory. *Prog. Oceanogr.* **45**, 1–38.

Osborne, A. R., Serio, M., Bergamasco, L. & Cavaleri, L. 1998 Solitons, cnoidal waves and nonlinear interactions in shallow-water ocean surface waves. *Physica* D **123**, 64–81.

Redekopp, L. G. 2000 Boussinesq theory for internal wave evolution in confined basins. In *Proc. 5th Intl Symp. on Stratified Flows* (ed. G. A. Lawrence, R. Pieters & N. Yonemitsu), vol. 1, pp. 367–372. University of British Columbia.

Renouard, D. P., Seabra-Santos, F. J. & Temperville, A. M. 1985 Experimental study of the generation, damping and reflexion of a solitary wave. *Dyn. Atmos. Oceans* **9**, 341–358.

Sandstrom, H. & Elliott, J. A. 1984 Internal tide and solitons on the Scotian Shelf: a nutrient pump at work. *J. Geophys. Res.* **89**, 6415–6426.

Segur, H. & Hammack, J. L. 1982 Soliton models of long internal waves. *J. Fluid Mech.* **118**, 285–304.

Spigel, R. H. & Imberger, J. 1980 The classification of mixed-layer dynamics in lakes of small to medium size. *J. Phys. Oceanogr*. **10**, 1104–1121.

Thorpe, S. A., Hall, A. & Crofts, I. 1972 The internal surge in Loch Ness. *Nature* **237**, 96–98.

Weidman, P. D. & Maxworthy, T. 1978 Experiments on strong interactions between solitary waves. *J. Fluid Mech.* **85**, 417–431.

Wiegand, R. C. & Carmack, E. 1986 The climatology of internal waves in a deep temperate lake. *J. Geophys. Res.* **91**, 3951–3958.